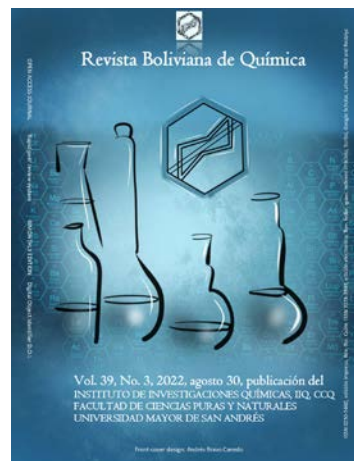# SYNTHESIS OF SILICOALUMINATE MESOPOROUS SUPPORT BY THE ATRANO ROUTE, MORPHOLOGICAL AND ACIDITY PROPERTIES OF THE MESOCELLULAR FOAM, MCF, FOR COBALT CATALYSTS DESIGN

Full original article   *Peer-reviewed*

Mauricio Claure Zeballos[1,2,*], Fátima L. Pardo Tarifa[1], Luis G. Lopez N.[1,2], Saúl Cabrera M.[1,2](†)

1. Laboratorio de Ciencia de Materiales, Instituto de Investigaciones Químicas IIQ, Department of Chemical Sciences, School of Pure and Natural Sciences FCPN, Universidad Mayor de San Andrés UMSA, P.O. Box 303, Calle Andrés Bello s/n-Edificio IIQ, Ciudad Universitaria Cota Cota, Phone +59122795878, La Paz, Bolivia, http://cienciasquimicas.umsa.bo/

2. Instituto del Gas Natural IGN, Universidad Mayor de San Andrés UMSA, P.O. Box 303, Calle Andrés Bello s/n-Edificio IIQ, Ciudad Universitaria Cota Cota, Phone +59122772269, La Paz, Bolivia. sicyt.umsa.bo/unidades/contactoInstituto/103

ABSTRACT

The synthesis of silicoalumina mesoporous supports was carried out by the atran route. The supports obtained showed high homogeneity in the aluminum dispersion, a large surface area and a narrow pore size distribution. The synthesized mesoporous mesocellular foam (MCF) supports contain 5%, 10% and 15% Al2O3 in the SiO2 matrix. 12% cobalt was added to these mesostructured supports by the incipient wetness impregnation method. These materials were characterized by Nitrogen adsorption (BET-BJH), Scanning Electron Microscopy (SEM), X-Ray Diffraction (XRD), Temperature Programmed Reduction of H2 (TPR), and Temperature Programmed Desorption of NH3. (TPD). According to the structural properties of these catalysts, a promising application in Fischer-Tropsch (FTS) syntheses is identified..

*Correspondent autor: mauricio.clze@gmail.com

RESUMEN

Se realizó la síntesis de soportes mesoporosos de silicoalumina por la ruta del atrano. Los soportes obtenidos mostraron alta homogeneidad en la dispersión de aluminio, un gran área superficial y una estrecha distribución del tamaño de poro. Los soportes de espuma mesocelular mesoporosa (MCF) sintetizados contienen 5%, 10% y 15% de Al_2O_3 en la matriz de SiO_2. A estos soportes mesoestructurados se les añadió 12% de cobalto por el método de impregnación por humedad incipiente. Estos materiales fueron caracterizados por los métodos de adsorción de Nitrógeno (BET-BJH), Microscopía Electrónica de Barrido (SEM), Difracción de Rayos X (DRX), Reducción a Temperatura Programada de H_2 (TPR), y Desorción a Temperatura Programada de NH_3 (TPD). De acuerdo a las propiedades estructurales de estos catalizadores, se identifica una aplicación prometedora en las síntesis de Fischer-Tropsch (FTS).

INTRODUCTION

Through GTL (Gas to Liquid) technology it is possible to obtain derivatives such as gasoline, gas oil, kerosene, higher alcohols, diesel, among others, using natural gas as raw material. For this, natural gas is initially directed to the Steam Reforming process, using nickel catalysts where synthesis gas (CO and H_2) is obtained. Then, the synthesis gas is directed to the Fischer-Tropsch process where paraffinic chains are obtained using Cobalt catalysts. Finally, the products with larger carbon chains (waxes) are treated in a hydrocracking process. For the Fischer Tropsch process, the commercial catalysts are based on Cobalt and Iron. However, on a large scale, other metals such as Ruthenium are discarded due to its high cost and low availability. Nickel produces a large amount of methane. Iron has a high selectivity to light hydrocarbons and olefins. Cobalt has a high selectivity to heavy and paraffinic hydrocarbons, from which Diesel can be obtained. The supports typically used for the (FTS) processes are alumina, amorphous silica and titanium oxide (TiO_2). However, new catalytic supports are currently being studied, such as ordered silicoaluminate mesoporous supports (1-Dimensional, 2-Dimensional and 3-Dimensional), carbon nanotubes, and silicon carbides, among others. The advantage of these new supports compared to conventional ones is the high specific surface area to disperse the active sites (cobalt) and their intrinsic uniform pore size distribution.

Various ordered mesoporous materials are reported in literature [1]. MCM-41 (Mobil Composition of Matter, No. 41) is a 1-Dimensional mesoporous material with average pore size of 1.5 to 10nm [2-4].. SBA-15 (Santa Barbara Amorphous, No. 15) is a 2-Dimensional mesoporous material with an average pore size of 2 to 10nm [4,5]. MCF (MesoCellular Foam) is a 1-Dimensional mesoporous material with average pore size of 5 to 50nm [6,7]. In recent years, the addition of aluminum into mesoporous cellular foam materials has been studied [5,8], however, few studies focused on comparing the physical-chemical properties of these materials when aluminum is incorporated in the mesoporous structure. The incorporation of aluminum into mesoporous supports can improve the support stability for longer periods of time [6,8].

In this work, the synthesis of ordered mesoporous silicoaluminate supports like MCF was developed by the "atrane route" [1,9,10] incorporating 5%, 10% and 15% w/w of aluminum. Finally, 12% w/w of cobalt was added by the incipient wetness impregnation method. All the materials were characterized by physical-chemical methods and compared with each other. Then, we studied the relationships among certain properties, specially the type of acidity (Lewis and Brønsted) and the degree of reducibility, with the desired properties of the supports for their application in the Fischer-Tropsch synthesis.

The two main goals of this work are to, first, broaden the application of mesoporous silica-alumina synthesis by the atrane route to other structures, particularly 3D mesocellular structures, and then, to investigate the effect of acidity, pore structure, and silica-alumina size on the cobalt catalyst as a whole.

EXPERIMENTAL

Synthesis of the silatrane-alumatrane complex: MCF precursor

Before the synthesis of mesoporous supports MCF, the atrane complex of silicon and aluminum was prepared according to S. Cabrera et al. [9]. Initially, triethanolamine ($TEAH_3$) was heated to 140°C, then, tetraethyl orthosilicate (TEOS) and Aluminium isopropoxide (AIP) were added. After that, it was heated to 140°C, keeping this temperature for 30 minutes.

MCF with 10% of structural aluminum

The synthesis method is similar to SBA-15Al reported by Pardo-Tarifa et al. and Li et al. [1,5] with the following modifications: The amount of ammonium fluoride is 2.67g and the amount of 1,3,5-trimethylbenzene (TMB) is 16.8 ml. The molar composition of the reagent mixture is: SiO_2: Al_2O_3: $TEAH_3$: P-123: TMB: NH_4F: HCl: H_2O equal to 0.89: 0.054: 3.44: 0.019: 4.38: 0.87: 5.76: 178.90. The support thus obtained was named as MCF10Al.

Synthesis of MCF with different content of structural aluminum: 5% Al, 10% Al and 15% Al

For the MCF-type silicoaluminate series with different proportions of Al_2O_3, the synthesis was performed in a similar manner as the MCF synthesis mentioned above. The molar composition is the same as in the MCF10Al support, however, the molar ratio Si: Al for the MCF5Al support is 0.94: 0.030 and for the MCF15 support is 0.83: 0.087.

Cobalt impregnation on mesoporous supports

For all the synthesized mesoporous silatrane-alumatrane supports, cobalt was added by the incipient wetness impregnation method [5,11]. A nominal weight percentage of 12% Co was added to the supports from an aqueous solution of cobalt nitrate. The impregnated supports were dried at 70°C overnight, then, they were calcined as follow: till 120°C for 4 hours, heated up till 220°C for 4 hours, and finally heated up till 350°C for 6 hours. All the mentioned steps were done at a rate of 2°C/min. Thus, the catalysts obtained were named as Co/MCF5Al, Co/MCF10Al and Co/MCF15Al.

Support and catalyst characterization

The nitrogen adsorption/desorption was analyzed at a constant temperature, 77 K, in a surface analyzer Autosorb iQ from Quantachrome Instruments. The surface area was obtained by means of the BET (Brunauer-Emmet-Teller) method, and the volume and pore size distribution were obtained by means of the BJH (Barrett-Joyner-Halenda) method. The SEM images were obtained in a Philips XL-30 Electron Microscope Equipment SEM that operates at a voltage of 15 KV with last minute resolution of 1 μm and a magnification range of 200X to 5000X. The X-ray diffraction analysis (XRD) was performed on a model of the equipment from Panalytical X'Pert Pro X-ray reflectometer, equipped with a goniometer and a Cu lamp (Kα line, λ=1.5406 Å). The analysis program includes a sweep angle: $10° \leq 2\theta \leq 90°$.

The analysis of desorption of ammonia at a programmed temperature, TPD, was carried out in a ChemBET TPR/TPD from Quantachrome Instruments. About 0.1g of sample was used in a U-quartz tube, the sample was degassed with a Nitrogen flux (N_2 5.0 ultra-High Purity) of 70 ml/min at 250°C for about 1 hour. This sample was then activated with a flow of Helium (He 5.0 ultra-High Purity) of 70 ml/min with a heating ramp of 10°C/min up to 500°C, maintaining this temperature for 30 minutes. Subsequently, the temperature is lowered to 100 °C and a flow of ammonia (5% V/V of NH_3/He) of 50 ml/min is passed, allowing the ammonia to adsorb in the sample for 1 hour. The physically adsorbed ammonia was then removed for 1 hour at 100°C with a He flow. Finally, the TPD analysis with helium flow of 70 ml/min was performed, increasing the temperature 10 °C/min up to 800°C and keeping it at this temperature for approximately 60 min. For the TPD analysis of the catalysts, prior analysis, the catalyst was activated with dilute Hydrogen flux (5% V/V H_2/N_2) of 70 ml/min with a temperature ramp of 10 °C/min up to 500 °C and kept at this temperature for 20 min before the analysis.

The TPR programmed temperature reduction analysis was carried out on a ChemBET TPR/TPD equipment from Quantachrome instruments. About 0.1 g of sample was used in a U-quartz tube. The sample was degassed with nitrogen flow (N_2 5.0 ultra-High Purity) of 70 ml/min at 250°C for about 1 hour. Afterwards, the temperature was lowered to 20°C and then, the TPR analysis of the cobalt catalysts was carried out with diluted hydrogen flow (5% V/V H_2/N_2) of 70 ml/min with a temperature ramp of 10°C/min up to 900°C and kept at this temperature for 20min.

RESULTS AND DISCUSSION

*Mesoporous cellular Foam (MCF) with different Alumina content*

Nitrogen Physisorption (BET-BJH)

The adsorption/desorption isotherms of MCF in different aluminum content supports are shown in figure 1. The shape of the isotherms is divided into four parts: The first part of the isotherm is at a relative pressure (P°/P) between 0 and 0.15. The second part of the isotherm is at a relative pressure (P°/P) of 0.15 to 0.7 for MCF5Al and MCF10Al; and 0.15 to 0.6 for MCF15Al, which belongs to the formation of multilayers. The third part of the isotherm is at a relative pressure (P°/P) from: 0.7 to 0.94 for the MCF10Al support; from 0.7 to 0.96 for MCF5Al support and from 0.6 to 0.9 for the MCF15Al support. According to the hysteresis loop type [12] (see figure 2). It is of the H1 and H2 type. These isotherms tend slightly to the H3 type, generating a deformation of the isotherm compared to the MCF support isotherm that may be due to the content of Aluminum. Finally, it is possible to observe the last part of the isotherm, which is at a relative pressure (P°/P) between 0.94 and 0.96 to 1. The shape of this last part of the isotherm is similar to the H1 for MCF10Al and MCF15Al; and similar to H3 for MCF5Al.

As can be seen in figure 1, the slope of the hysteresis of the MCF10Al support may be due to the existence of tetrahedral Aluminum inside the structure, and to octahedral aluminum that would be found in the commonly called extra-framework Aluminum (EFA) [13-15]. This wider variation in nitrogen capillary condensation (hysteresis inclination) implies a greater extension in the pore size distribution and in turn, this also affects the result of pore volume and surface area.

The supports of the type MCF-Al present two types of porosity, window and cell. These refer to the internal diameter of the pore (cell) and the diameter of entrance to the pore (window). Besides, in general, the MCF (without Al) supports have 3D spherical pores, moderately high surface area, and uniform pore size distribution [4,7,16]. Thus, the specific surface area of the MCF-Al support is smaller than MCF because it has a larger pore sizes. However, the specific area and pore size distribution has a variation according to the amount of aluminum added. In table 1 the MCF5Al support has the largest pore size distribution, and the smallest specific surface area. Inversely, the MCF15Al support has the smallest pore size distribution, and the largest specific area, because of their smallest pores. This shows a greater distortion of the mesostructure when a higher proportion of aluminum is added to the support.
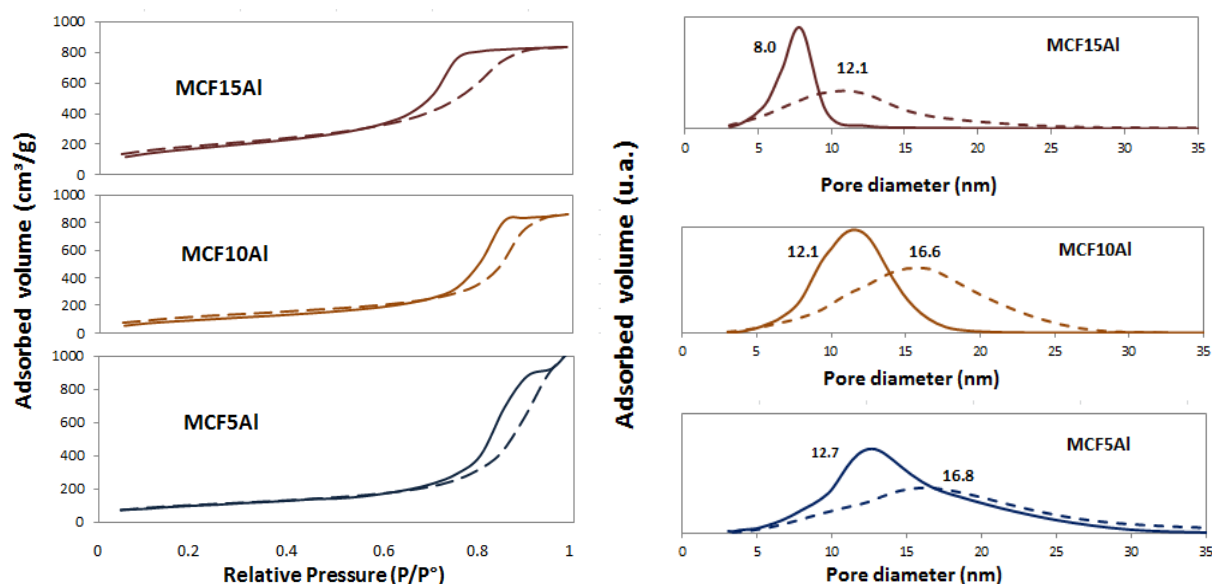
Figure 1. N_2 *Adsorption-Desorption isotherms and pore size distribution of a series of MCF supports containing alumina. The surface area (see table 3) of the supports has the following sequence: MCF15Al> MCF10Al> MCF5Al; 643.4 m²/g; 408.5 m² /g; 349.4 m²/g, respectively. The window pore size distribution of the supports (see table 3) MCF5Al> MCF10Al > MCF15Al are: 12.6 nm; 12.1 nm and 8.2 nm respectively. In the same way, the cell pore size distribution of the supports MCF5Al> MCF10Al > MCF15Al are: 16.8nm, 15.9nm and 12.5nm.*
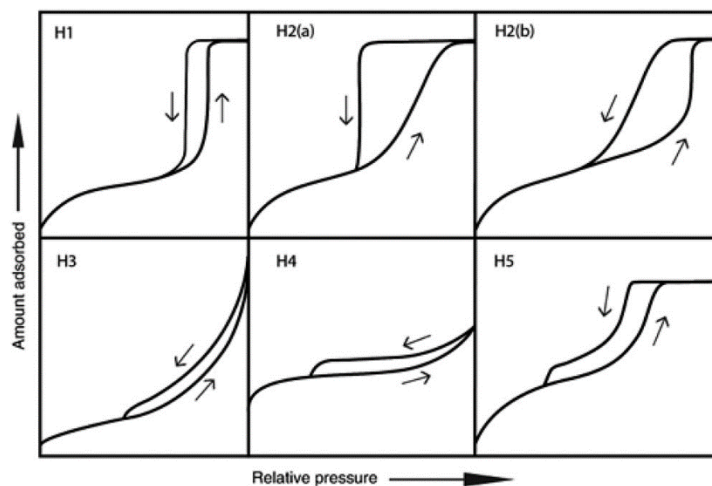
Small Angle X-Ray Diffraccion (XRD)

The XRD patterns of mesoporous MCF supports with aluminum content are shown in figure 3. For the mesostructured supports type MCF-Al, the characteristic signal of the MCF support is observed at the 2θ (2 theta) ≈ 0.5° position. These results agree with the results of the nitrogen adsorption analysis (BET-BJH). However, there is some displacement of the signal from right to left when the amount of Aluminum in the structure increases from

5% for the MCF5Al support up to 15% for the MCF15Al support. This could also show that while the amount of aluminum increases in the structure, the ordering of the pores decreases.

Table 1. *Surface area, pore volume and pore size distribution of MCF5Al, MCF10Al, MCF15Al,*

Material	BET surface area (m²/g)	Pore volume (cm³/g)	Pore diameter (window) (nm)	Pore diamenter (cell) (nm)
MCF5Al	349.4	1.59	12.6	16.8
MCF10Al	408.5	1.60	12.1	15.9
MCF15Al	643.4	1.20	8.2	12.5

Figure 2. IUPAC Classification of adsorption-desorption hysteresis loops [12, 17].
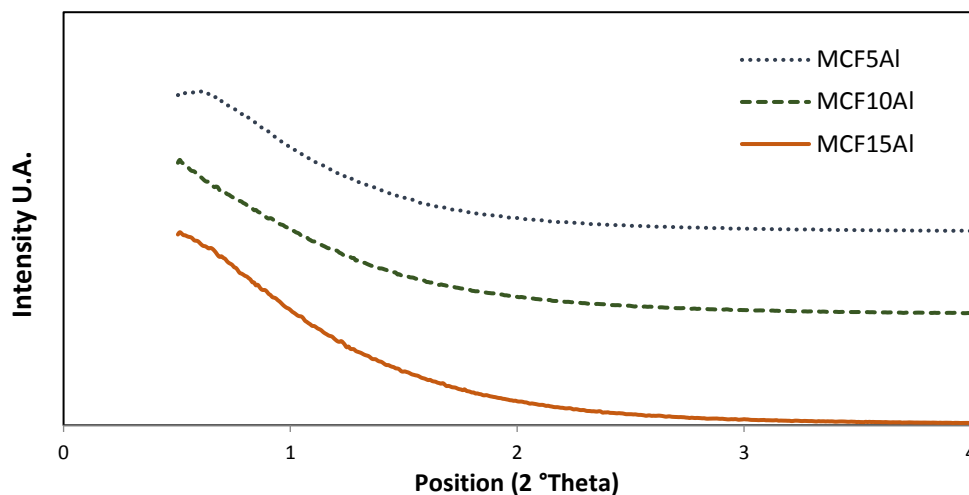
Figure 3. *XRD patterns of MCF Supports with 2θ from 0.5-4.0 MCF5Al, MCF10Al y MCF15Al*

Temperature Programed Desorption (TPD)

TPD of mesoporous MCF5Al, MCF10Al and MCF15Al

The deconvolution of TPD profiles for the mesoporous silicoaluminate MCF-Al different supports are presented in Figure 4. Figure 4a, 4b, and 4c show the deconvolution profiles of MCF5Al, MCF10Al, and MCF15Al, respectively. Each figure shows three principal signals that were identified and compared based in the literature [8,15,18-20]. The first signal at 222, 215, and 242 °C, respectively, which might correspond to Brönsted and Lewis weak acid sites such as: the silanols (Si-O-H) with low number of aluminum atoms near to the silicon atom (NNN's) respectively and the species seen in figure 5(d) from Weitkamp, J. et. al [15].
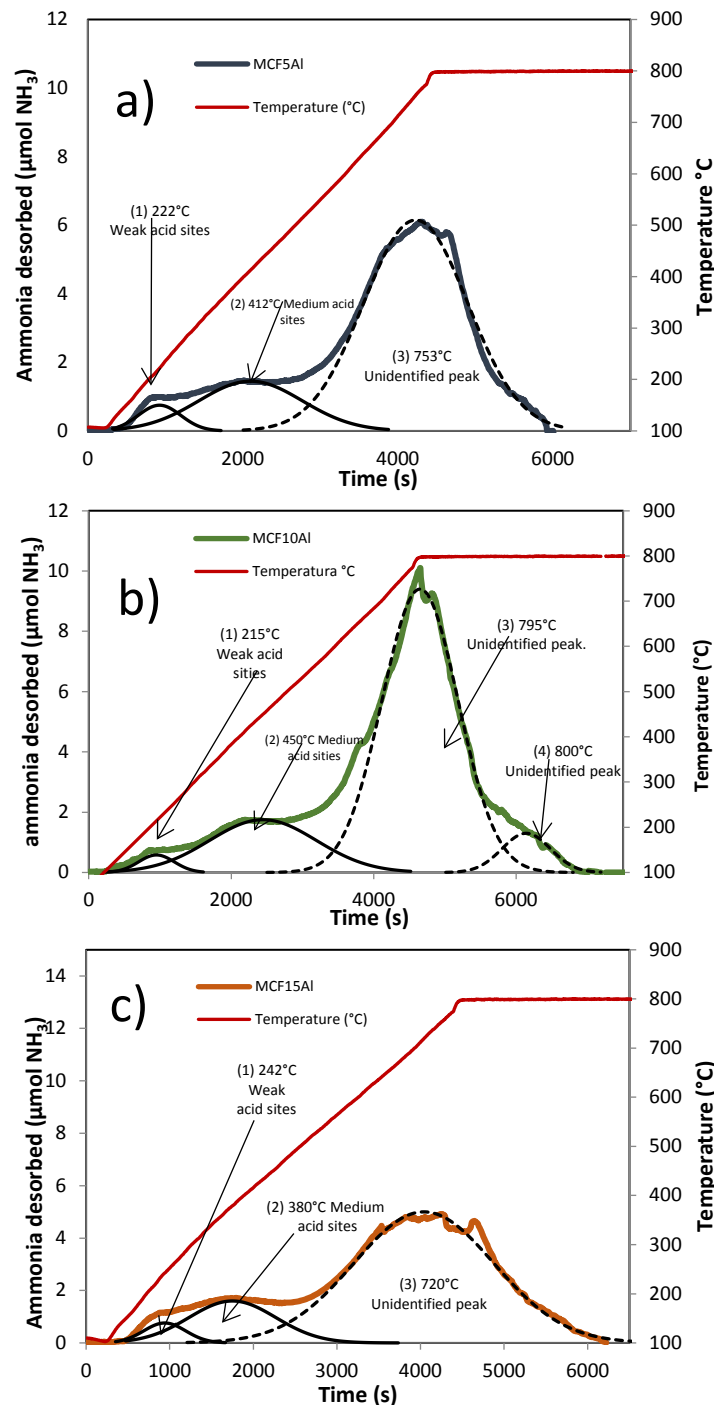

Figure 4. *Temperature-Programmed Desorption TPD Profile of support: a) MCF5Al, b) MCF10Al and c) MCF15Al*

The second signal at 412ºC, 450°C and 380ºC corresponds to the deconvolution profiles of MCF5Al, MCF10Al, and MCF15Al, respectively. They may correspond to Brönsted and Lewis medium acid sites such as: the silanols

(Si-O-H) with medium number of aluminum atoms near to the silicon atom (NNN's) and alumina species Extra-framework Aluminum such as AlO(OH) (see figure 5(c)) respectively. The third signal at 753°C, 795ºC and 720ºC, respectively, corresponds to an unidentified peak that may be strong acidity, which might agree to Brønsted and Lewis strong acid sites. These sites may be Si-O-H, Si-OH-Al bonds type (see figure 5(a) and 6(b)) with high number of aluminum atoms near to the silicon atom (NNN's), and species extra framework such as AlO^+, $Al(OH)^{2+}$, respectively. Finally, an unidentified signal at 800°C is found for MCF10Al only.
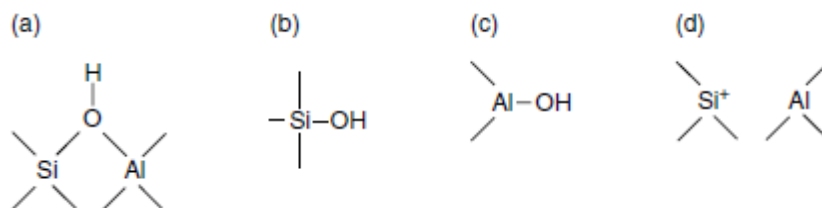

Figure 5. *Scheme representing the different types of hydroxyl groups and acid sites in a silicoaluminate* [15].

Table 2 shows the study database of the deconvolution of the TPD analyzes of the mesoporous supports according to the amount of aluminum in the mesoporous MCF type (MCF5Al, MCF10Al and MCF15Al). There, the silicon to aluminum ratio was 16.2; 7.6 and 4.8 for MCF5Al, MCF10Al and MCF15Al, respectively. The supports have a higher amount of ammonia desorbed per gram according to the following order MCF10Al> MCF5Al> MCM15Al. The dispersion of acid sites per square meter of mesoporous support area (μmol NH_3/m^2) has the following order MCF10Al> MCF5Al> MCM15Al. The percentage of accessibility of the acid sites ((μmol NH_3 desorbed/μmol of Al in the sample) * 100) has the following sequence from highest to lowest MCF5Al> MCF10Al> MCM15Al.

Table 2. *Adsorption capacity of the mesoporous supports and catalysts type MCF*

Material	Adsorption of NH_3 per support mass (μmol/g) according to type of acidity			Total adsorption (μmol/g)	Dispersion[1] (μmol NH_3/m^2)	% accessibility[2]	Metal adsorption[3] (μmol/m²)
	Weak acid	Medium acid	Strong acid				
MCF5Al	10,2	48,1	206,6	264,9	0,76	27	-
MCF10Al	7,2	65,5	252	324,8	0,8	16,6	-
MCF15Al	9,4	41,3	209,8	260,5	0,40	8,9	-

[1]*μmol of NH_3 per gram/ specific surface area (g/m^2);* [2]*Aluminium in the surface of support/total aluminum;* [3]*μmol of metal acidity sites per gram of catalyst*

Hydrolysis and condensation

The hydrolysis and condensation process for MCFAl materials with different concentrations of aluminum are typically performed in acidic medium (pH = 1-2). Pluronic-123 triblock micelles are formed by liquid crystal mechanisms or by cooperative arrangement, depending on system conditions and surfactant concentration. A micelle expander agent is added so that the shape of the surfactant micelles passes from hexagonal cylinders in 2D to 3D spheres [7,12]. Generally, the difference in hydrolysis and condensation rates with aluminum and silicon complexed with alkoxides is very high. However, when it comes to silatrane and alumantrane complexes, the hydrolysis and condensation rates decrease considerably, mainly due to steric hindrance. [2,9]. This would facilitate a greater uniformity of deposition of hydrolyzed species on the surface of the surfactant. Although the surfactant of P-123 is anionic, it is characterized by a negatively charged surface [6]. This property causes regions with higher densities of positive charges of hydrolyzed aluminum and silicon species to be attracted to this surface.

Acid sites formation

Thus, in this way, the negative charges on the surface of the micelles act similarly to a nucleophilic attack on the positively charged areas of the hydrolyzed species of the Aluminum and silicon atoms. Consequently, with less amount of Aluminum content, there will be less strength. This is because there will not be strong charges of an anion as such, but with a negative charge density, the interaction will be similar to a weak adsorption (physisorption). Thus, the hydrolyzed species will be attracted and adsorbed to these surfaces. As a result, high

amounts of strong Lewis and Brønsted acid sites will be obtained. However, by restructuring and stabilizing the charges, weak and medium acid sites of Lewis and Brønsted can also be formed, but in smaller proportions.

Dried and calcined

Drying and calcining are also important stages so that mesostructured spherical 3D pores do not suffer damage or cracking, due to rough thermal conditions. In addition, it is at this stage, where the intensity and type of acidity on the surface finish forming.

Textural and structural characterization

Characterization was carried out by the methods of Nitrogen Adsorption (BET-BJH), and X-ray Diffraction at low angles (DRX). The spherical structure in 3D of the support could be evidenced, in addition, it was observed that the pore size distribution and the adsorption and desorption isotherm correspond to the MCF type material [5-6,10]. However, there is some distortion of the uniformity of the pores. This may be due to the fact that during the deposition of hydrolyzed Silicon and Aluminum species, there is a rearrangement of the species due to the formation of Aluminum in the tetrahedral and octahedral state. Thus, this rearrangement deforms the uniformity of the porous structure [3,5-6]. When the Si/Al ratio decreases, there is a greater formation of octahedral aluminum on the surface, while increasing a greater number of extra-framework aluminum species. This further distorts the uniformity of the pores of the support.

According to the Ammonia Programmed Temperature Desorption (TPD) analysis, a high formation of strong acid sites of Brønsted and Lewis can be evidenced. In addition, a lower proportion of strong Lewis and Brønsted acids can be observed. The MCF10Al supports have a higher proportion of total acidity than the MCF5Al and MCF15Al supports. With low Al contents, the concentration of strong Brønsted acid sites, which are attributed to tetrahedral aluminum, increases with growing Al amounts. At higher Al contents, however, the number of strong acid sites decreases again. Furthermore, at low Al Contents, the amount of desorbed ammonia increases with growing content of aluminum. With increasing Al contents, the total amount of desorbed ammonia reaches a maximum value when the content of Al_2O_3 is approximately 10%. A further increase of the aluminum content, which is accompanied by structural losses, causes a distinct decrease of ammonia desorption. This might be due to the existence of an acidity limit achieved due to the Al Content. These results are similar with Kosslick, H et. al [6].

Cobalt catalysts on silicate aluminates: MCF with different Alumina content

Nitrogen Phisisorption (BET-BJH)

MCF5Al and Co/MCF5Al

The adsorption/desorption isotherms of MCF5Al and Co/MCF5Al with 12% of Co content are shown in figure 6. The shape of the isotherms is divided into four parts: The first part of the isotherm is at a relative pressure (P°/P) between 0 and 0.15. The second part of the isotherm is at a relative pressure (P°/P) of 0.15 to 0.7 for MCF5Al; and 0.15 to 0.68 for Co/MCF5Al, which belongs to the formation of multilayers. The third part of the isotherm is at a relative pressure (P°/P) of 0.7 to 0.96 for the MCF5Al support; and 0.68 to 0.9 for Co/MCF5Al catalyst. The hysteresis loop types are of the H1 and H2 type. These isotherms tend slightly to the H3 type. Finally, the last part of the isotherm is at a relative pressure (P°/P) between 0.96 and 0.9 to 1. This ending is similar to the H1 for MCF10Al, Co/MCF10Al, MCF15Al and Co/MCF15Al; and H3 for MCF5Al and Co/MCF5Al.

MCF10Al and Co/MCF10Al

The adsorption/desorption isotherms of MCF10Al and Co/MCF10Al with 12% of Co content are shown in figure 6. There are four parts that the isotherms form: The initial part of the isotherm is at a relative pressure (P°/P) between 0 and 0.15. The second part of the isotherm is at a relative pressure (P°/P) of 0.15 to 0.7 for MCF10Al; and 0.15 to 0.55 for Co/MCF10Al, which belongs to the formation of multilayers. The third part of the isotherm is at a relative pressure (P°/P) of 0.7 to 0.94 for the MCF10Al support; and 0.55 to 0.85 for Co/MCF10Al catalyst. The hysteresis loop type is of the H1 and H2 type. Finally, the last part of the isotherm is at a relative pressure (P°/P) between 0.94 and 0.85 to 1. This isotherm ending is similar to the H1 for both MCF10Al and Co/MCF10Al.

MCF15Al and Co/MCF15Al

The adsorption/desorption isotherms of MCF15Al and Co/MCF15Al with 12% of Co content are shown in figure 6. The shape of the isotherms is divided into four parts: The first part of the isotherm is at a relative pressure (P°/P) between 0 and 0.15. The second part of the isotherm is at a relative pressure (P°/P) of 0.15 to 0.6 for MCF15Al; and 0.15 to 0.67 which belongs to the formation of multilayers. The third part of the isotherm is at a relative pressure (P°/P) between: 0.6 and 0.9 for the MCF15Al support; and between 0.67 and 0.94 for the Co/MCF15Al. In this part, the hysteresis loop type is of the H1 and H2 type, which tend slightly to the H3 type. Finally, the last part of the isotherm, which is at a relative pressure (P°/P) between 0.9 and 0.94 to 1, has terminations that are similar to the H1 type.

As in the MCF-Al type supports, the inclination of the hysteresis of the Co/MCF-Al catalysts may be due to the existence of tetrahedral aluminum that is inside the structure, and to octahedral extra-framework aluminum [8,15,18,20]. In addition, the cobalt has an influence on the morphological nature of the pores of the catalyst. This affects the specific surface area and the pore size distribution. A wider variation in nitrogen capillary condensation (hysteresis inclination) implies a greater extension in the pore size distribution, and in turn, this also affects the results of pore volume and surface area [4].

As previously, the influence of the Al content on the textural properties of the MCF-Al type supports was observed. Similarly, when cobalt is added in the form of oxide, the surface area and the pore size distribution vary (see table 3). For the Co/MCF15Al catalyst, the pores of the MCF15Al support are smaller. This would imply that the Co_3O_4 particles could have covered a larger number of small pores of the support and the larger pores might have been left mostly free. For this reason, the average pore size distribution increases and the specific surface area decreases. For the Co/MCF10Al catalyst compared to the fresh MCF10Al support, the specific surface area increases and the pore size distribution decreases. This may be due to the pore size that is larger and some pores are partially covered, increasing the surface area and decreasing the pore size distribution. In the case of the Co/MCF5Al catalyst compared to the fresh MCF5Al support, this phenomenon is similar to Co/MCF10Al. However, this material has pores of a larger size, thus, decreasing the number of pores totally blocked.
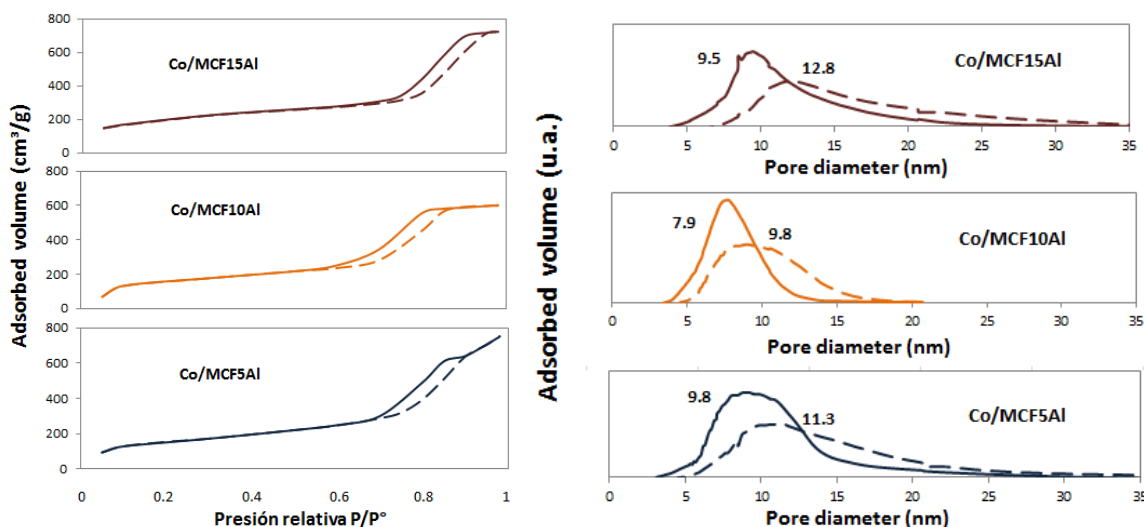
Figure 6. N_2 Adsorption-Desorption isotherms and pore size distribution of supports and catalysts of alumina content MCF series. a) Adsorption isotherms and pore size distribution of supports. b) Adsorption isotherms and pore size distribution of catalysts

In table 3 and according to figure 6, a summary of the results of the nitrogen desorption analysis of the cobalt catalysts Co/MCF5Al, Co/MCF10Al and Co/MCF15Al can be observed. The surface area, the pore volume, the internal pore size distribution are shown. The average window pore sizes of Co/MCF5Al, Co/MCF10Al and Co/MCF15Al are 9.8 nm; 7.9 nm and 9.5 nm respectively. The average internal pore sizes of Co/MCF5Al, Co/MCF10Al and Co/MCF15Al are 11.3 nm; 9.8 nm and 12.8 nm, respectively. The surface area calculated by the BET method, for Co/MCF5Al, Co/MCF10Al and Co/MCF15Al is 414.7 m^2/g; 422.1 m^2/g and 538.9 m^2/g, respectively.

Table 3. *Surface area, pore volume and pore size distribution of MCF5Al, MCF10Al, MCF15Al, Co/MCF5Al, Co/MCF10Al and Co/MCF15Al*

Material	BET surface area (m²/g)	Pore volume (cm³/g)	Pore diameter (window) (nm)	Pore diamenter (cell) (nm)
MCF5Al	349.4	1.59	12.6	16.8
MCF10Al	408.5	1.60	12.1	15.9
MCF15Al	643.4	1.20	8.2	12.5
Co/MCF5Al	414.7	1.09	9.8	11.3
Co/MCF10Al	422.1	0.91	7.9	9.8
Co/MCF15Al	538.9	1.11	9.5	12.8

X-Ray Diffraccion (XRD)

X-Ray Diffraction of cobalt supported catalysts

Figure 7 shows the XRD patterns of the cobalt support catalysts in silicoaluminate mesoporous, which are Co/MCF5Al, Co/MCF10Al, Co/MCF15Al. In each of these materials the presence of cobalt oxide Co_3O_4 is observed as the only crystalline phase of cobalt, with signals at angles 2θ (2 theta) ≈ 31.1°; 36.9°, 45.0°; 59.4° and 65.4°. These reflection signals are associated with the planes (2 2 0), (3 1 1), (4 0 0), (5 1 1) and (4 4 0) respectively [4,21-22], and these correspond to the cubic system centered on the face of the spinel Co_3O_4 [4,11]. The average crystallite size of Co_3O_4 and CoO were calculated using the Scherrer equation [1,5]. The Cobalt Co/MCF5Al catalyst has the most intense and sharp cobalt oxide characteristic signals compared to the Co/MCF10Al and Co/MCF15Al catalyst. Moreover, the Co/MCF10Al catalyst has the cobalt oxide (Co_3O_4) characteristic signals more intense and acute than the Co/MCF15Al catalyst. This could indicate that the catalysts have a crystalline domain size of cobalt particles according to the following sequence from highest to lowest: Co/MCF5Al> Co/MCF10Al > Co/MCF15Al. The most intense signal for these materials is at 2θ ≈ 36.9°. This peak is associated with the plane (3 1 1) [13]. Figure 7 and table 4 show the comparative sequence: Co/MCF5Al> Co/MCF10Al> Co/MCF15Al.
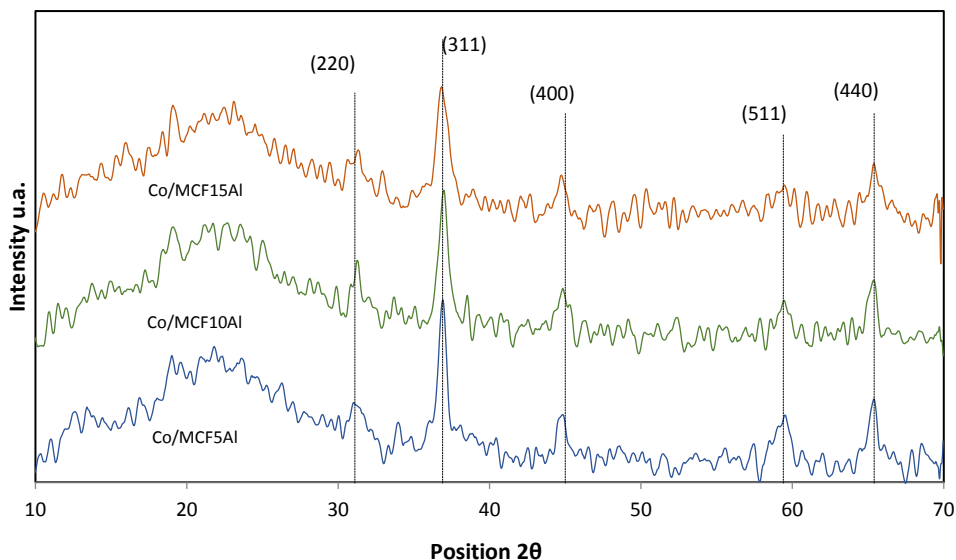
Figure 7. *XRD patterns of cobalt catalysts with 2θ from 10-70: Co/MCF5Al, Co/MCF10Al y Co/MCF15Al*

In table 4 and according to figure 7, the crystalline microdomain size of the cobalt particles found in the mesoporous silicoaluminate supports is observed. This parameter was calculated with the Scherrer equation [22]

which is represented as the diameter of the cobalt crystals in nanometers (nm). Figure 7 shows the cobalt catalysts Co/MCF5Al, Co/MCF10Al and Co/MCF15Al.

The crystalline microdomain size increased sequence is directly proportional to the increase in the pore size distribution of the mesoporous supports (See table 3. The microdomain crystalline size sequence of Co_3O_4 is as follows: Co/MCF5Al> Co/MCF10Al> Co/MCF15Al: 17.7nm> 13.3nm> 9,8nm, respectively. The microdomain crystalline size sequence of Co^0 is as follows: Co/MCF5Al> Co/MCF10Al> Co/MCF15Al; 13.3nm> 10.0nm> 9.8nm respectively. However, the crystal size distribution of Co_3O_4 and Co^0 is larger than the average size of each of the mesostructure types. This may be due to the particle size distribution of Co_3O_4 and Co^0 that increases because there are particles of the largest metal clusters found on the surface of the support particles. [14]

Table 4. *Crystallite size from XRD analysis of Cobalt particles of the Co/MCF5Al, Co/MCF10Al and Co/MCF15Al catalysts*

cobalt catalyst	D(Co_3O_4)	D ($Co°$)*
Co/MCF5Al	17.7	13.3
Co/MCF10Al	13.3	10.0
Co/MCF15Al	13.1	9.8

* $d(Co^0)=0,75d(Co_3O_4)$. [14]

Temperature Programmed Reduction (TPR)

Figure 8 shows the signs of TPR profiles, of the Co/MCF5Al, Co/MCF10Al and Co/MCF15Al catalysts. The reduction signals of the three catalysts are divided into two well-marked regions, the first at low temperatures between 237°C and 603°C, and the second is between 610°C and 900°C.

The signals at low temperatures represent the reduction reactions of Co_3O_4 to CoO and from CoO to Co^0. The signals at high temperatures represent the cobalt oxide and minor phases such as cobalt silicates and cobalt silicoaluminates that have high interaction with the support [14,22]. The deconvolution at low temperature shows a signal for the reduction from Co_3O_4 to CoO in agreement to [11,21-22], and two signals for the reduction from CoO to Co^0. CoO is reduced in two stages; In one hand, this is due to the reduction of CoO on the surface of the cobalt particles (weak metal-support interactions); in the other hand, it is due to the reduction of CoO that is close to or those CoO that has an interaction with the surface of the support (strong metal-support interactions) [6,14].

The consumption of H_2 in the region of low temperature follows as: Co/MCF5Al > Co/MCF10Al > Co/MC15Al. The signal for the Co/MCF5Al is displaced at lower temperatures compared to the other two catalysts. The reduction signal at low temperatures of the Co/MCF5Al catalyst represents the highest H_2 consumption and also has the widest peak and a high temperature displacement. From the consumption of H_2 in the region at high temperature, the catalysts are ordered as: Co/MCF5Al> Co/MCF10Al> Co/MCF15Al.

Regarding the extent of each reduction reaction, the temperature at which the reduction from Co_3O_4 to CoO occurs is similar in the three catalysts as shown in figure 8. More CoO is reduced to Co^0 in the Co/MCF15Al catalyst as in contrast to Co/MCF10Al and Co/MCF15Al catalysts (see table 5), specially, in the reduction at low temperature (L). Thus, the reducibility degree decreases in the following order: Co/MCF15Al> Co/MCF10Al> Co/MCF15Al. The latter is an important parameter for the application in catalytic synthesis such as the Fischer-Tropsch synthesis, where the higher reducibility the higher the activity of the catalyst.

Table 5 and Figure 8 show the summary of the H_2 consumption data of the integrals of the conversion of the TPR results of the cobalt catalysts Co/MCF5Al, Co/MCF10Al and Co/MCF15Al. For the reduction of Co_3O_4 →CoO, there are no differences in brands between the three catalysts. For the CoO→ Co^0 reduction at low temperatures (L), there is an order for the H_2 consumption of the catalysts as follows: Co/MCF5Al> Co/MCF10Al> Co/MCF15Al. For the CoO →Co^0 reduction at high temperatures (H) there is an order for H_2 consumption of the catalysts as follows: Co/MCF5Al> Co/MCF10Al> Co/MCF15Al. For the cobalt silicoaluminous zone, it does not have a marked sequence that is the following: Co/MCF5Al> Co/MCF15Al> Co/MCF10Al. The cobalt catalyst Co/MCF5Al has the highest degree of reduction of 54.1%, followed by the Co/MCF10Al catalyst with 44.1%, and the Co/MCF15Al catalyst that has a lower reduction percentage of 29.8%.
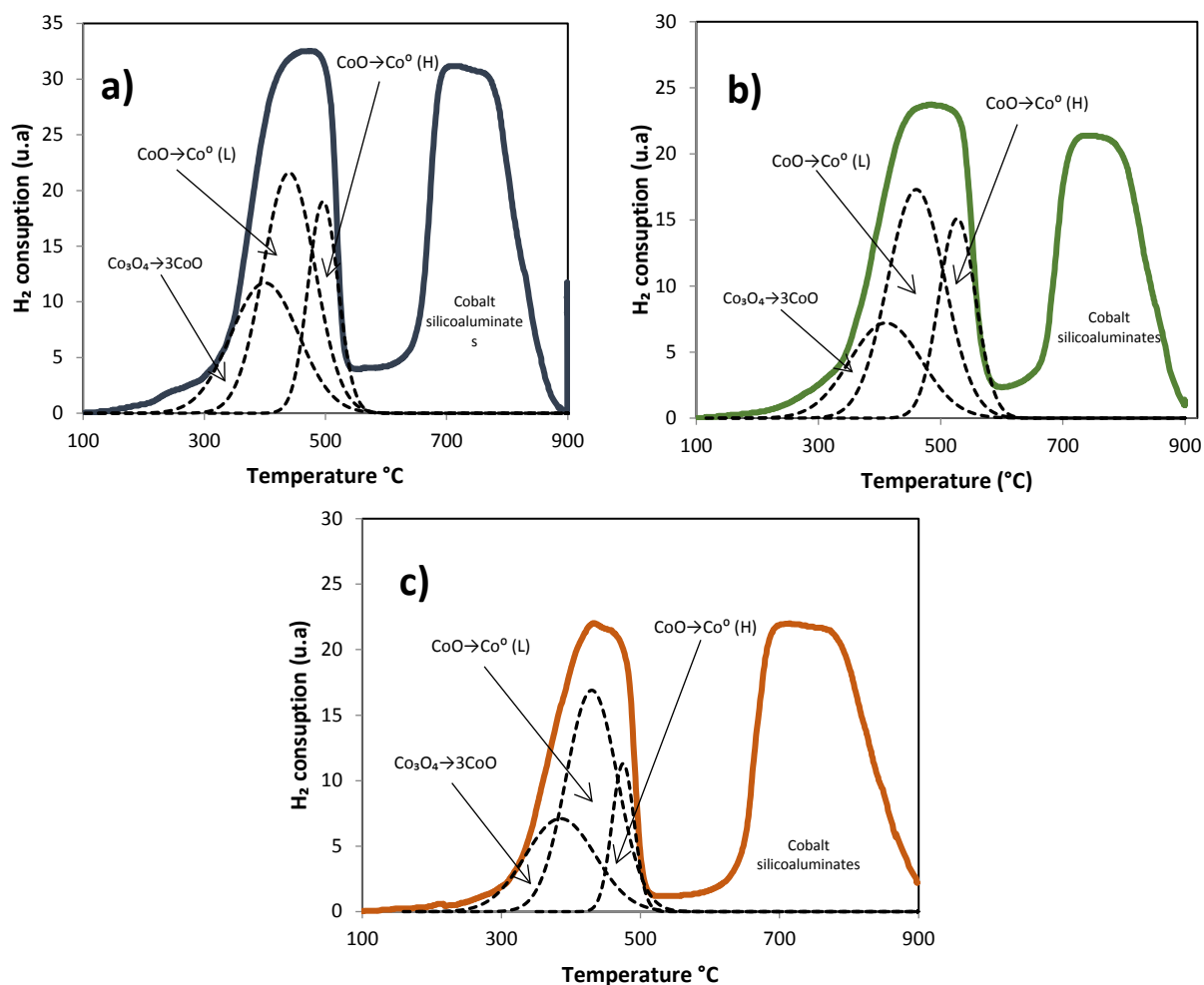
Figure 8. *Temperature- Programmed Profile for reduction of catalysts: a)Co/MCF5Al, b)Co/MCF10Al, c)Co/MCF15Al*

Table 5. *Hydrogen consumption of cobalt catalysts: Co/MCF5Al, Co/MCF10Al and Co/MCF15Al*

Material	Consumption of H_2 per catalyst mass ($\mu mol\ H_2/g$) depending on the type of reaction				% Reducibility degree
	$Co_2O_3 \rightarrow CoO$	$CoO \rightarrow Co^o(L)$	$CoO \rightarrow Co^o(H)$	Co Silicoaluminates	
Co/MCF5Al	1,11	1,59	0,82	2,98	54,1
Co/MCF10Al	0,71	1,38	0,77	2,09	44,1
Co/MCF15Al	0,59	1,04	0,30	2,47	29,8

Temperature-Desorption Programmed (TPD)

a) TPD of mesoporous Co/MCF5Al catalyst

The deconvolution of TPD profiles for the mesoporous silicoaluminate MCF5Al support and Co/MCF15Al catalyst (figure 9a) shows similar TPD profiles for both materials. For MCF5Al at low temperature ($\leq 500°C$), three signal are identified as compared to literature: at 222°C a weak acidity, and at 412°C a medium acidity. At high temperature ($\geq 500°C$) an unidentified peak that could correspond to strong acidity is found at 753°C. The latter signal is notably increased by the presence of Cobalt (Co/MCF5Al catalyst), which might be attributable to Lewis weak, medium and strong acidity of Co^0 [13]. Also, when cobalt is added to MCF5Al, the total amount of acid sites is increased by 2.5 fold as is shown in table 8. In addition, the dispersion of acid sites is increased by approximately twice when cobalt is added.

b) TPD of mesoporous Co/MCF10Al catalyst

The deconvolution of TPD profiles for the mesoporous silicoaluminate MCF10Al support and Co/MCF10Al catalysts (see figure 9b) shows similar TPD profiles for both materials. For MCF10Al, there are three signals that are identified as compared to literature: at 215°C a weak acidity, at 450°C a medium acidity, and at 795°C a strong acidity peak. The strong acidity peak at 795 °C is an unidentified peak. Moreover, an unidentified signal at 800°C is found. The latter signal is notably increased by the presence of Cobalt (Co/MCFAl catalyst), which might be attributable to Lewis strong acidity of Co° [6]. Also, when cobalt is added to MCF10Al, the total amount of acid sites are increased by 50% fold as is shown in table 4. In addition, the dispersion of acid sites is increased by approximately a 50% when cobalt is added.

c) TPD of mesoporous Co/MCF15Al catalyst

The deconvolution of TPD profiles for the mesoporous silicoaluminate MCF15Al support and Co/MCF15Al catalysts (see figure 9c) shows similar TPD profiles for both materials. For MCF15Al, there are three identified signals as compared to literature: at 242°C a weak acidity, at 380°C a medium acidity, and at 720°C an unidentified peak that it may be strong acidity. The latter signal is markedly increased by the presence of Cobalt (Co/MCF15Al catalyst), which might be explained by a Lewis weak, medium and strong acidity of Co^0 [13]. Also, when cobalt is added to MCF15, the total amount of acid sites is increased by 2.5 fold as is shown in table 4. In addition, the dispersion of acid sites is increased by approximately three times when cobalt is added.

Table 6 shows the study database of the deconvolution of the TPD analysis of the mesoporous supports according to the amount of aluminum in the mesoporous MCF type (MCF5Al, MCF10Al and MCF15Al). The silicon/aluminum ratio was 16.2; 7.6 and 4.8 for MCF5Al, MCF10Al and MCF15Al respectively. The supports have a higher amount of ammonia desorbed per gram according to the following order MCF10Al> MCF5Al> MCM15Al. The dispersion of acid sites per square meter of mesoporous support area ($\mu mol\ NH_3/m^2$) has the following order MCF10Al> MCF5Al> MCM15Al. The percentage of accessibility of the acid sites (($\mu mol\ NH^3$ desorbed/μmol of Al in the sample) * 100) has the following sequence from highest to lowest MCF5Al> MCF10Al> MCM15Al.

Table 6. *Adsorption capacity of the mesoporous supports and catalysts type MCF*

Material	Adsorption of NH₃ per support mass (µmol/g) according to type of acidity			Total adsorption (µmol/g)	Dispersion¹ (µmol NH₃/m²)	% accessibility²	Metal adsorption³ (µmol/m²)
	Weak acid	Medium acid	Strong acid				
MCF5Al	10,2	48,1	206,6	264,9	0,76	27	-
MCF10Al	7,2	65,5	252	324,8	0,8	16,6	-
MCF15Al	9,4	41,3	209,8	260,5	0,40	8,9	-
Co/MCF5Al				669,4	1,61	-	404,5
Co/MCF10Al				530,3	1,26	-	205,5
Co/MCF15Al				704,2	1,31	-	443,7

¹μmol of NH_3 per gram/ specific surface area (g/m^2); ²Aluminium in the support surface/ total aluminum; ³μmol of metal acidity sites per gram of catalyst

For the series of supports and catalysts type MCF with aluminum variation (MCF5Al, MCF10Al and MCF15Al), the results of nitrogen physisorption show high specific surface area, and a narrow pore size distribution in the order of the mesopores. According to these results, these materials could be suitable as support for Fisher Tropsch catalysts, and catalytic cracking among others. The variation of surface area and pore size distribution in this series depends on the amount of Aluminum inserted in the matrix. In the XRD diffractograms of the cobalt catalysts in this series, it is observed that the Cobalt particles were inserted homogeneously in the supports, since there is a single phase of cobalt in the surface of the matrix which is the double oxide of cobalt (Co_3O_4). This property is good for catalysis because the reduction of this cobalt phase is expected at low temperatures.
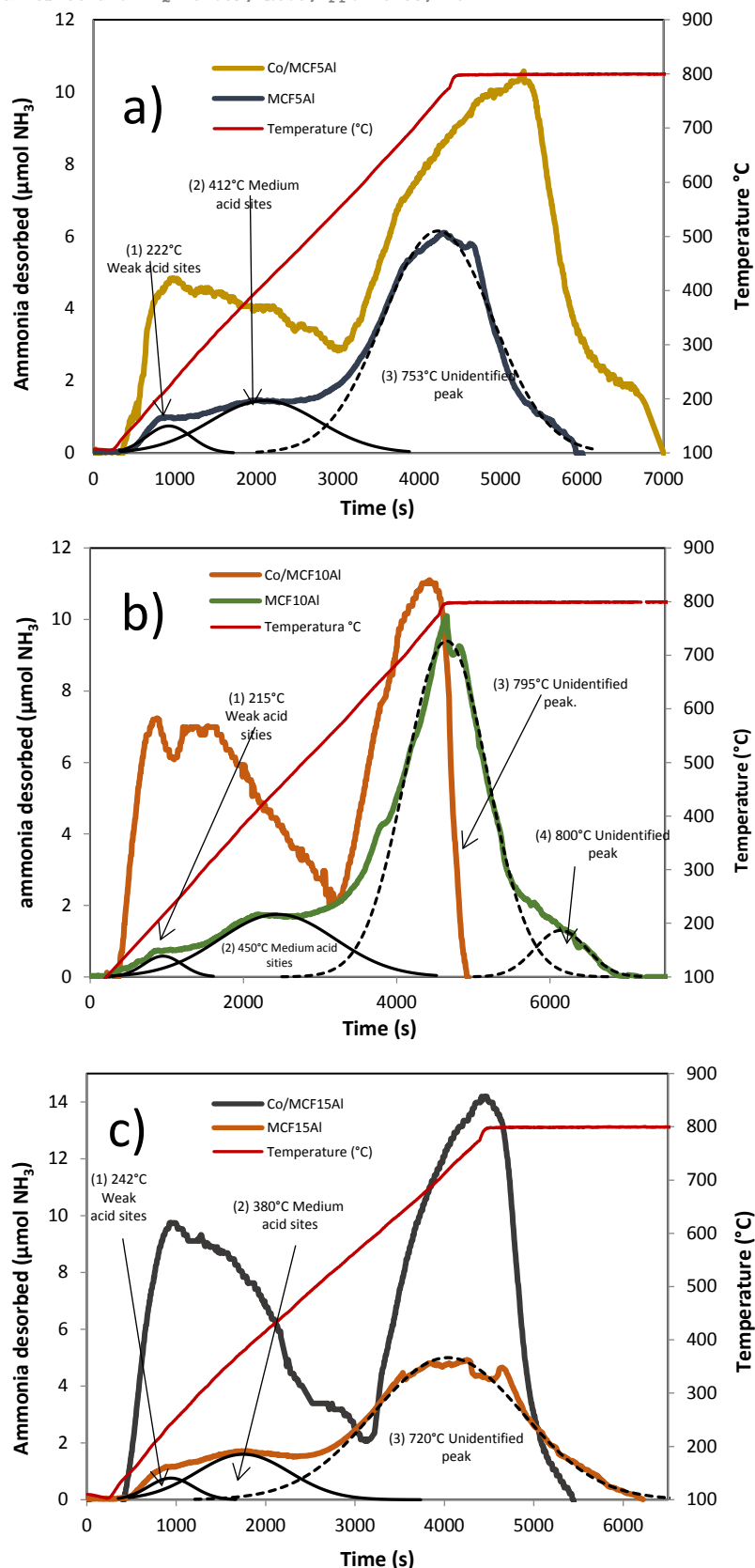
Figure 9. *Desorption Temperature-Programmed TPD Profile of support and catalysts: a) MCF5Al and Co/MCF5Al, b)MCF10Al and Co/MCF10Al, c)MCF15Al and Co/MCF15Al*

The mesoporous supports and catalysts synthesized by the atrane route show different weak, medium and strong acid species of Lewis and Brønsted, depending on the amount of Aluminum added (MCF5Al, MCF10Al and MCF15Al). Addition of cobalt to these matrices results in an increase of the acidity of the medium and weak acids of Lewis, which varies according to the type of mesostructure. These Lewis acids are due to the presence of Co^0 that could be related to the catalytic performance of the cobalt active sites. The TPR reduction profiles of the 12% Cobalt catalysts are similar to the series according to mesoporous type. However, the Co/MCF5Al catalyst has a greater degree of relative reducibility. The total amount of reduction depends on the type of support and the amount of aluminum inserted in the matrix. This property is important for Fischer-Tropsch Synthesis.

CONCLUSION

New mesoporous silicoaluminate supports synthesized by the atrane route type MCFAl with high specific surface area and with a narrow pore size distribution were obtained. According to Nitrogen Adsorption results (BET-BJH). The MCF-Al support shows high surface area, homogeneous pore size distribution and considerable total acidity. However, the hysteresis of the isotherm loops and the mesoporous structure are deformed when the aluminum content increases. When cobalt is added to the support, the mesostructured structure is further deformed.

Cobalt catalysts were obtained, by the incipient wet impregnation method, on the mesoporous supports of silicoaluminates. According to X-ray diffraction analysis (XRD), a single phase of oxide was identified as cobalt oxide (Co_3O_4). The crystalline microdomain size of the cobalt catalysts presents a range between 10 and 17.7nm. These values were calculated by the Scherrer equation.

The TPR programmed temperature reduction analysis of hydrogen was carried out for all the mesoporous catalyst supports. The Co/MCF5Al catalyst obtained the highest proportion of degree of reducibility reaching up to 54.1%; the Co/MCF/10Al catalyst has the greater displacement at higher temperatures in CoO reactions: $CoO \rightarrow Co^0$ (L) and (H).

By means of TPD technique, the total acidity of the mesoporous supports could be calculated.in the same manner. It was calculated the type and quantity of each of the acids present in the mesoporous supports, the dispersion of the acidity and the accessibility of these. In addition, TPD analysis of the cobalt catalysts was performed, where an increase in the weak, medium and strong Lewis acids was found. These Lewis acids of the cobalt active sites may be related to the Fischer-Tropsch catalytic activity. The understanding of this type of correlation as well as its control through the synthesis method is of vital importance to obtain new catalysts with better performances.

Finally, the properties of these supports and catalysts were observed, such as: high degree of reducibility; uniform pore size distribution; high surface area; high degree of acidity in the support and the catalyst; cobalt crystallite distribution around 10 nm averages; and considerable reducibility of Cobalt at low relative temperatures. Therefore, these materials are considered promising for their use in heterogeneous catalysis tests in Fisher-Tropsch reactions.

AKNOWLEDGEMENTS

REFERENCES

1. Pardo-Tarifa, F., Montes, V., Claure, M., Cabrera, S., Kusar, H., Marinas, A., Boutonnet, M. **2017**, Silica with 3D Mesocellular Pore Structure Used as Support for Cobalt Fischer-Tropsch Catalyst, S*ynthesis and Catalysis: Open Access*, *2*(3), 11. DOI: 10.4172/2574-0431.100017
2. Cabrera, S., El Haskouri, Guillem, C., Latorre, J., Beltrán-Porter, A., Beltrán-Porter, D., Dolores-Marcos, M., Amorós, P. **2000**, Generalised syntheses of ordered mesoporous oxides: the atrane route, *Solid State Sciences 2*, 405–420. DOI: https://doi.org/10.1016/S1293-2558(00)00152-7
3. Chen, C-Y., Li, H-X., Davis, M.E. **1993**, Studies on mesoporous materials: I. Synthesis and characterization of MCM-41, *Microporous Materials*, *2*, 17-26. DOI: 10.1016/0927-6513(93)80058-3
4. Santos, G.A., Santos, C.M.B., da Silva, S.W., Urquieta-González, E.A., Confessori Sartoratto, P.P. **2012**, Sol–gel synthesis of silica–cobalt composites by employing Co3O4 colloidal dispersions, *Colloids and Surfaces A: Physicochem. Eng. Aspects, 395*, 217– 224. DOI: https://doi.org/10.1016/j.colsurfa.2011.12.033
5. Li, Y., Zhang, W., Zhang, L., Yang, Q., Wei, Z., Feng, Z., Li, C. **2004**, Direct Synthesis of Al-SBA-15 Mesoporous Materials via Hydrolysis-Controlled Approach, *J. Phys. Chem. B.*, *108*(28), 9739-9744. DOI: https://doi.org/10.1021/jp049824j

6. Wei, L., Zhao, Y., Zhang, Y., Liu, C., Hong, J., Xiong, H., Li, J. **2016**, Fischer–Tropsch synthesis over a 3D foamed MCF silica support: Toward a more open porous network of cobalt catalysts, J*ournal of Catalysis 340*, 205–218. DOI: https://doi.org/10.1016/j.jcat.2016.04.019

7. Cao, L., Kruk, M. **2010**, Synthesis of large-pore SBA-15 silica from tetramethyl orthosilicate using triisopropylbenzene as micelle expander, *Colloids and Surfaces A: Physicochemical and Engineering Aspects*, *357*(1–3), 91-96. DOI: https://doi.org/10.1016/j.colsurfa.2009.09.019

8. Kosslick, H., Lischke, G., Parlitz, B., Storek, W., Fricke, R. **1999**, Acidity and active sites of Al-MCM-41, *Applied Catalysis A: General*, *184*(1), 49-60. DOI: https://doi.org/10.1016/S0926-860X(99)00078-2

9. Cabrera, S. **1999**, Química en medios organizados para la obtención de nuevas alúminas, aluminosilicatos y ALPO's mesoporosos con tamaño de poro modulable, (PhD Tesis), Universitat de Valéncia, Valencia, España, retrieved from https://dialnet.unirioja.es/servlet/tesis?codigo=225426

10. Pardo-Tarifa, F. **2017**, Cobalt catalyst supports for Fischer-Tropsch synthesis, (PhD Thesis), KTH Royal Institute of Technology, Stockholm, Sweden, retrieved from http://www.diva-portal.org/smash/get/diva2:1146405/FULLTEXT02.pdf

11. González, O., Pérez, H., Navarro, P., Almeida, L.C., Pacheco, J.G., Montes, M. **2009**, Use of different mesostructured materials based on silica as cobalt supports for the Fischer–Tropsch synthesis, *Catalysis Today*, *148*(1-2), 140–147. DOI: https://doi.org/10.1016/j.cattod.2009.03.030

12. Zhao, D., Wan, Y., Zhou, W. Ordered Mesoporous Materials, Wiley-VCH Verlag GmbH & Co. KGaA, **2013**, Singapore, pp. 138-144. DOI: 10.1002/9783527647866

13. Claure, M. **2017**, Obtención de silicoaluminatos mesoporosos por la ruta de los atranos evaluando sus propiedades acido/base y redox para identificar su potencial aplicación como matrices en procesos catalíticos, (MSc tesis), Instituto de Investigaciones Químicas (IIQ), Universidad Mayor de San Andrés (UMSA), La Paz, Bolivia, retrieved from https://repositorio.umsa.bo/handle/123456789/17880

14. Liu, Y., Hanaoka, T., Miyazawa, T., Murata, K., Okabe, K., Sakanishi, K. **2009**, Fischer–Tropsch synthesis in slurry-phase reactors over Mn- and Zr-modified Co/SiO_2 catalysts, *Fuel Processing Technology*, *90*(7-8), 901–908. DOI: https://doi.org/10.1016/j.fuproc.2009.04.004

15. Weitkamp, J., Hunger, M. Acid and Base Catalysis On Zeolites. Institute of Chemical Technology, University of Stuttgart, Stuttgart, Germany. DOI:10.1016/S0167-2991(07)80810-X

16. Wattanathana, W., Laobuthee, **2015**, A. Simple cerium-triethanolamine complex: Synthesis, characterization, thermal decomposition and its application to prepare ceria support for platinum catalysts used in methane steam reforming, *Journal of Molecular Structure*, *1089*(9–15, DOI: doi.org/10.1016/j.molstruc.2015.02.010

17. Schlumberger, C., Thommes, M. **2021**, Characterization of hierarchically ordered porous materials by physisorption and mercury porosimetry—A tutorial review, *Advanced Materials Interfaces, 8*(4), 2002181. DOI: https://doi.org/10.1002/admi.202002181

18. Xu, B., Bordiga, S., Roel Prins a , van Bokhoven J. **2007**, Effect of framework Si/Al ratio and extra-framework aluminum on the catalytic activity of Y zeolite, *Applied Catalysis A: General 333*, 245–253, *Applied Catalysis A: General 333*(2), 245-253. DOI:10.1016/j.apcata.2007.09.018

19. Zanjanchi M.A, Hemmati, M. **2004**, Verification of extra-framework aluminum in zeolite L by acetylacetone. *Materials Chemistry and Physics, 85*, 334–339. doi.org/10.1016/j.matchemphys.2004.01.010

20. Silaghi, M., Chizallet, C., Raybaud, P. **2016**, Dealumination mechanisms of zeolites and extra-framework aluminum confinement. *Journal of Catalysis, Elsevier*, *339*, 242-255. doi.org/10.1016/j.jcat.2016.04.021

21. Martínez, A., Lopez, C. **2006,** Fischer-Tropsch catalysts based on cobalt supported on ordered mesoporous silicas, *Revista Mexicana de Ingeniería Química*, *5*(3), 167-177.

22. Song, D., Li, J. **2006**, Effect of catalyst pore size on the catalytic performance of silica supported cobalt Fischer-Tropsch catalysts, *Journal of Molecular Catalysis A: Chemical*, *247*(1-2), 206–212. DOI: https://doi.org/10.1016/j.molcata.2005.11.021